HHS Public Access

Author manuscript

Magn Reson Med. Author manuscript; available in PMC 2023 September 01.

Published in final edited form as:

Magn Reson Med. 2022 September ; 88(3): 1081–1097. doi:10.1002/mrm.29271.

Selective excitation localized by the Bloch-Siegert shift and a B_1^+ gradient

Jonathan B. Martin[1,2], **Sai Abitha Srinivas**[1,2], **Christopher E. Vaughn**[1,2], **Heng Sun**[2], **Mark A. Griswold**[3,4], **William A. Grissom**[1,2,5]

[1]Vanderbilt University Institute of Imaging Science, Nashville, Tennessee, USA

[2]Department of Biomedical Engineering, Vanderbilt University, Nashville, Tennessee, USA

[3]Department of Radiology, Case Western Reserve University, Cleveland, Ohio, USA

[4]Department of Biomedical Engineering, Case Western Reserve University, Cleveland, Ohio, USA

[5]Department of Electrical Engineering, Vanderbilt University, Nashville, Tennessee, USA

Abstract

Purpose: To perform B_1^+-selective excitation using the Bloch-Siegert shift for spatial localization.

Theory and Methods: A B_1^+-selective excitation is produced by an RF pulse consisting of two summed component pulses: an off-resonant pulse that induces a B_1^+-dependent Bloch-Siegert frequency shift and a frequency-selective excitation pulse. The passband of the pulse can be tailored by adjusting the frequency content of the frequency-selective pulse, as in conventional B_0 gradient-localized excitation. Fine magnetization profile control is achieved by using the Shinnar-Le Roux algorithm to design the frequency-selective excitation pulse. Simulations analyzed the pulses' robustness to off-resonance, their suitability for multi-echo spin echo pulse sequences, and how their performance compares to that of rotating-frame selective excitation pulses. The pulses were evaluated experimentally on a 47.5 mT MRI scanner using an RF gradient transmit coil. Multiphoton resonances produced by the pulses were characterized and their distribution across B_1^+ predicted.

Results—With correction for varying B_1^+ across the desired profile, the proposed pulses produced selective excitation with the specified profile characteristics. The pulses were robust against off-resonance and RF amplifier distortion, and suitable for multi-echo pulse sequences. Experimental profiles closely matched simulated patterns.

Conclusion—The Bloch-Siegert shift can be used to perform B_0-gradient-free selective excitation, enabling the excitation of slices or slabs in RF gradient-encoded MRI.

Address correspondence to: Jonathan B. Martin, 1161 21st Ave. South, MCN AA-1105, Nashville, TN 37232-2310, jonathan.b.martin@vanderbilt.edu.

Keywords

RF pulse design; Selective RF excitation; Bloch-Siegert shift; RF encoded MRI; Multiphoton; low-field MRI

Introduction

Gradients in the static B_0 magnetic field are used in nearly all modern magnetic resonance imaging systems. Although B_0 gradients are versatile tools capable of performing a variety of functions in the imaging process, their use also creates substantial challenges. Gradient hardware is expensive and occupies a large portion of the scanner's bore, constraining scanner design; gradient switching is loud and induces peripheral nerve stimulation, compromising patient comfort; and eddy currents and concomitant non-linear magnetic fields induced by gradients require correction to prevent image artifacts (1, 2).

Imaging with magnitude or phase gradients of the RF transmit field $\left(B_1^+\right)$ rather than the static B_0 magnetic field has long been investigated as an alternative to B_0 gradient encoding (3–6). B_1^+ gradients can be switched in near-negligible time without acoustic noise, eddy currents, or peripheral nerve stimulation resulting from large dB/dt (7). However, replacing B_0 gradients with RF magnitude gradients in an imaging system introduces a new challenge: how to spatially localize excitation utilizing only the RF transmit field. A number of methods exist which exploit an inhomogeneous transmit field for spatial discrimination, such as early techniques for localized spectroscopy in B_1^+ gradients utilizing composite 180° hard pulses (8–10). These pulse trains achieve a rudimentary degree of spatial localization but require multiple FID acquisitions to define the ROI and do not provide strict profile definition. Another approach, the related depth pulse sequence technique, requires a smaller number of FID acquisitions and is somewhat more robust to off-resonance than composite pulses, but similarly provides only minimal control over the excitation profile (11). A third method proposed by Hoult is rotating-frame B_1^+-selective excitation (RFSE) by means of an RF pulse with constant $B_{1,x}$ and modulated $B_{1,y}$ (12). These pulses selectively excite magnetization based on the strength of the $B_{1,x}$ component. The selectivity of the rotating frame method was improved over time (13–15), and a later recasting of the problem as a rotated Shinnar-Le Roux (SLR) design enabled pulse designers to meet target slice profile characteristics in B_1^+ (16). Although this most recent method provides fine control of the excitation profile, these pulses face some practical challenges, including unintended excitation at low B_1^+ with off-resonance and sensitivity to RF amplifier distortions due to the pulses' strict envelope area requirements (16).

This work describes a class of B_1^+-selective RF pulses that use the Bloch-Siegert shift (17) to localize excitation. The Bloch-Siegert shift is a temporary shift in the resonance frequency of a nucleus, produced by the application of an off-resonant RF field. The size of the frequency shift induced by the off-resonant RF field depends on the frequency offset of the applied pulse and the strength of the RF field. This property has allowed the Bloch-Siegert

shift to be used for mapping B_1^+ fields in MRI (18) and calibrating decoupling field strength in NMR (19, 20). More recently, the phenomenon has been exploited as an encoding mechanism for B_0 gradient-free imaging (5, 21, 22). In this work, the Bloch-Siegert shift is used to localize excitation. Preliminary aspects of the pulse design algorithm were presented in Ref. (23).

The proposed B_1^+-selective pulses comprise the summation of 1) a far-off-resonant Bloch-Siegert frequency-shift-inducing pulse, and 2) a frequency-selective excitation pulse (Fig. 1a). The two pulses work in analog to the paired B_0 z-gradient and frequency-selective excitation pulse used in conventional imaging slice selection. The Bloch-Siegert pulse creates a nonlinear frequency gradient that varies with B_1^+ field strength, and the frequency-selective pulse is designed with a frequency passband that excites a range of B_1^+'s of interest (Fig. 1b). If the transmit coil generates a spatially inhomogeneous B_1^+ field, the B_1^+ selectivity of the summed pulse translates to spatial selectivity.

The primary resonance used for excitation by the proposed pulses is the Bloch Siegert-shifted single-photon resonance. However, the new pulse class is reliant on the simultaneous application of two off-resonant pulses in the xy plane, which also produces additional multiphoton resonances (24, 25). Although imaging techniques that use multiphoton resonances for excitation have recently been demonstrated (26), these additional resonances are here regarded as nuisances and their mitigation is discussed.

In the following, the design of the two component pulses that make up a Bloch-Siegert-localized B_1^+-selective excitation pulse is described. Although there are many feasible choices for both the off-resonant Bloch-Siegert-shift inducing pulse and the frequency-selective pulse, this work focuses on the promising combination of an amplitude- and frequency-swept off-resonant pulse and an SLR frequency-selective pulse which allows the designer to directly specify and analytically trade off pulse and B_1^+ profile parameters (27). Design of these two pulses is analytic, simple, and fast. Simulations show the pulses' suitability for selective excitation, inversion, and refocusing. Off-resonance behavior is simulated and shown to be predictable and similar to that of conventional spatially slice-selective excitation pulses, without the out-of-band excitation produced by the RFSE pulses of Ref (16). The pulses are also shown to have improved robustness against RF amplifier distortions over RFSE pulses. Selective excitation is experimentally demonstrated on a 47.5 mT MRI scanner with a gradient solenoid transmit-receive coil.

Theory

The design of a Bloch-Siegert B_1^+-selective excitation (BSSE) pulse comprises the design of two distinct component pulses: 1) an off-resonant pulse, $b_{bs}(t)$, which produces a B_1^+-dependent shift in resonant frequencies via the Bloch-Siegert effect, and 2) a frequency-selective SLR pulse, $b_{ex}(t)$, which excites a desired B_1^+ passband. Although these two pulses

could be transmitted by separate coils, we here assume that they are generated together by the same transmit coil, so they are complex-summed once individually designed, i.e.,

$$b_{total}(t) = b_{bs}(t) + b_{ex}(t).$$

Component Pulse 1: The Bloch-Siegert Shift-Inducing Pulse

In the absence of externally applied RF, the magnetic resonance frequency is the Larmor frequency, $\omega_0 = \gamma B_0$. If an RF field is applied with amplitude B_1^+ and frequency offset ω_{off} relative to ω_0, then a Bloch-Siegert frequency shift of the resonance is produced, given by (28):

$$\omega_{bs}\left(B_1^+, \omega_{off}\right) \approx -\omega_{off}\left(\sqrt{1 + \left(\frac{\gamma B_1^+}{\omega_{off}}\right)^2} - 1\right). \quad (1)$$

This shift is away from the frequency of the applied off-resonance RF, i.e., a positive ω_{off} results in a negative ω_{bs}.

The Bloch-Siegert shift-inducing pulse is defined as an amplitude- and phase-modulated function

$$b_{bs}(t) = A_{bs}(t)e^{i\phi_{bs}(t)},$$

where $\phi_{bs}(t) = \int_{-T/2}^{t} \Delta\omega_{rf}(t')dt'$ is the time integral of the pulse's time-varying frequency modulation $\Delta\omega_{rf}(t)$, and T is the pulse duration. For $A_{bs}(t)$ we use a Fermi pulse which was previously used in Ref. (18) to produce a large BS frequency shift with little out-of-band excitation. The Fermi envelope provides an additional benefit for this application: its plateau results in a constant ω_{bs} for the majority of the pulse duration, which simplifies the design of the $b_{ex}(t)$ pulse so long as $b_{ex}(t)$ is restricted to be nonzero only on the plateau. Thus for $A_{bs}(t)$ a normalized Fermi pulse is used which is centered at $t = 0$:

$$A_{bs}(t) = \frac{1}{1 + e^{\frac{|t| - t_0}{a}}}, \quad (2)$$

where t_0 and a are parameters with units of seconds that control the duration of the pulse and the width of the transition, respectively. The duration of this Fermi pulse is $T = 2t_0 + 13.81a$. To ensure that $b_{ex}(t)$ is only nonzero during the plateau when $A_{bs}(t) \approx 1$, we derive from Eq. 2 that t_0 should be set to:

$$t_0 = \frac{T_{ex}}{2} - a\ln\left(\frac{1}{A_{th}} - 1\right),$$

where T_{ex} is the duration of $b_{ex}(t)$ required to excite the desired bandwidth and A_{th} is a user-specified constant. This t_0 setting creates a central plateau in the Fermi envelope of duration T_{ex} with $A_{bs}(t) \geq A_{th}$. Herein, all pulse designs used $a = 6 \times 10^{-5}$ s and $A_{th} = 0.95$.

A modification is made to the conventional constant frequency-offset Fermi by starting and ending the pulse's FM waveform far-off resonance and sweeping adiabatically towards and away from the central constant frequency offset ω_{off}. This modification spin-locks the magnetization during the Fermi's amplitude sweeps, reducing undesired excitation by $A_{bs}(t)$ (29, 30). The analytic adiabatic sweep of Ref. (30) is used, with modification to allow for time-varying $A_{bs}(t)$. A frequency sweep adapted from the analytic adiabatic sweep of Ref. (30) is used, with modification to allow for time-varying $A_{bs}(t)$. The first half of the symmetric frequency sweep is given by:

$$\Delta\,\omega_{sweep}(t) = \frac{\gamma A_{bs}(t)}{\sqrt{\left(1 - \frac{\gamma A_{bs}(t)}{K} t_d\right)^{-2} - 1}}, \quad t \in (0, T/2),$$

where T is the duration of the full $A_{bs}(t)$ waveform, t_d is the hardware dwell time, and K is a design parameter which trades off the maximum offset of the frequency sweeps and undesired excitation by $A_{bs}(t)$. $K = 0.2$ was used for all pulses in this work, which produces a maximum frequency offset of ~10–30 kHz for a practical ω_{off} range of 5 − 20 kHz. The full FM waveform with constant frequency plateau ω_{off} is then given by:

$$\Delta\,\omega_{rf}(t) = \begin{cases} -\Delta\,\omega_{sweep}(t + T/2) + \max\left(\Delta\,\omega_{sweep}(t)\right) + \omega_{off}, & -T/2 < t < 0, \\ -\Delta\,\omega_{sweep}(T/2 - t) + \max\left(\Delta\,\omega_{sweep}(t)\right) + \omega_{off}, & 0 \leq t < T/2\,. \end{cases}$$

An example of an amplitude- and frequency-modulated $b_{bs}(t)$ is shown in Fig. 1a. Note that the frequency modulation of this pulse is positive for all t, producing a negative Bloch-Siegert shift for all B_1^+. As a result, the frequency-selective excitation pulse described in the next section is modulated to a negative frequency relative to Larmor, to excite the desired B_1^+ passband.

Component Pulse 2: The Frequency-Selective SLR Excitation Pulse

For a given desired passband between field strengths $B_{1,L}^+$ and $B_{1,H}^+$, the bandwidth of resonant frequencies that must be excited by the frequency selective SLR pulse $b_{ex}(t)$ is:

$$B = \omega_{bs}\left(B_{1,L}^+, \omega_{off}\right) - \omega_{bs}\left(B_{1,H}^+, \omega_{off}\right).$$

$b_{ex}(t)$ must further be frequency modulated to the center of the passband, which has frequency:

$$\omega_{cent} = \frac{1}{2}\left(\omega_{bs}\left(B_{1,L}^{+}, \omega_{off}\right) + \omega_{bs}\left(B_{1,H}^{+}, \omega_{off}\right)\right).$$

The Shinnar Le-Roux (SLR) pulse design algorithm is used to design $b_{ex}(t)$ since it allows for direct design of pulses to meet design constraints including bandwidth (B), duration (T_{ex}), flip angle (θ), transition width, and magnetization profile ripple (δ_1^e and δ_2^e) (27). Based on these parameters, SLR designs a pair of polynomials that are transformed to the discretized excitation pulse by the inverse SLR transform. Given the designer's choice of time-bandwidth product $T_{ex}B$, the duration of the excitation pulse T_{ex} is determined by B. The RF pulse output by SLR is interpolated to the target dwell time and scaled to produce the desired flip angle θ for the B_1^+ at its passband center, based on the relationship:

$$\theta = \gamma\ \Delta_t\ B_1^+(\omega_{cent}) \sum_{i=0}^{N-1} A_{ex}(t_i), \tag{3}$$

where Δ_t is the dwell time, N is the number of time points in the pulse, and $A_{ex}(t)$ is the baseband RF pulse waveform generated by SLR after interpolating it to the target dwell time. $B_1^+(\omega_{cent})$ is derived from Eq. 1 after rearranging it to give the B_1^+ producing a Bloch-Siegert shift of ω during an RF pulse with frequency offset $\omega_{off} > 0$:

$$B_1^+(\omega) \approx \frac{\omega_{off}}{\gamma}\sqrt{\left(1 - \frac{\omega}{\omega_{off}}\right)^2 - 1}\,. \tag{4}$$

After scaling $A_{ex}(t)$ to the desired flip angle, $b_{ex}(t)$ is obtained by frequency modulating it to ω_{cent}. The final pulse is then:

$$b_{ex}(t) = A_{ex}(t)e^{i\omega_{cent}t}.$$

Before summing $b_{ex}(t)$ with $b_{bs}(t)$, $b_{ex}(t)$ is zero-padded to match the full duration T of $b_{bs}(t)$. An example $b_{ex}(t)$ with $T_{ex}B = 4$ and $\theta = 90°$ is shown in Figure 1a.

However, under the assumption that both $b_{ex}(t)$ and $b_{total}(t)$ are played from the same transmit coil, $b_{ex}(t)$ will produce a sloped magnetization profile (or a distorted profile, in the case of 180° excitation) due to the fact that $b_{ex}(t)$ is played out slightly weaker than designed at passband locations where $B_1^+ < B_1^+(\omega_{cent})$ and slightly stronger than designed where $B_1^+ > B_1^+(\omega_{cent})$. The degree of distortion will depend on the width of the passband relative to its center, $\left(B_{1,H}^{+} - B_{1,L}^{+}\right)/B_1^+(\omega_{cent})$, and is therefore more pronounced for wide passbands and center positions closer to zero. Modifications can be made to the SLR algorithm to correct for these distortions, and the procedure adopted is outlined in Fig. 2a. For small-tip and 90° excitation, the distortion is approximately compensated by scaling the SLR algorithm's $B_N(\omega)$ polynomial by the inverse of the transmit field strength

corresponding to each frequency ω in the profile, with normalization to $B_1^+(\omega_{cent})$, prior to applying the inverse SLR transform:

$$B_N(\omega) \leftarrow \frac{B_1^+(\omega_{cent})}{B_1^+(\omega + \omega_{cent})} B_N(\omega).$$

For 180° inversion or refocusing, profile distortion cannot be corrected with this analytic method. Instead, an iterative optimization of the RF pulse is used to alleviate profile distortion caused by varying B_1^+ (described further in Methods).

Overall Pulse Design Procedure

The overall pulse design procedure is to first select the B_1^+ passband edges $B_{1,H}^+$ and $B_{1,L}^+$, the excitation pulse's SLR algorithm parameters and flip angle, and the BS pulse's frequency offset ω_{off}. With these parameters, the SLR pulse is designed, interpolated to the target dwell time, scaled to the desired flip angle, and frequency modulated to the center frequency ω_{cent} of the slice, yielding the pulse $b_{ex}(t)$. Knowing the duration T_{ex} of $b_{ex}(t)$ the BS pulse $b_{bs}(t)$ is calculated, $b_{ex}(t)$ is zero-padded to the same length as $b_{bs}(t)$, and the two pulses are complex-summed to obtain the total pulse $b_{total}(t) = b_{bs}(t) + b_{ex}(t)$. It should be noted that the choice of ω_{off} is critical to the performance of the pulse. Figure 3a shows the relationship between ω_{off} and total pulse duration. For all BSSE pulses duration is minimized by minimizing ω_{off} (which maximizes the Bloch-Siegert frequency gradient). However, as shown in Figure 3b, bringing ω_{off} too close to the Larmor resonance produces undesirable out-of-band excitation.

As in conventional B_0 gradient-selective excitations, at the end of a BSSE excitation pulse there will be a phase ramp across the slice that must be refocused if the slice dimension will not be resolved by subsequent spatial encoding. For BSSE pulses, the phase ramp depends on the $b_{ex}(t)$ pulse's isodelay and the K_{BS} of the $b_{bs}(t)$ pulse (18). A BSSE rewinding pulse can be constructed in the same manner as $b_{bs}(t)$, but with opposite frequency sign and a central constant frequency offset section with duration equal to the isodelay of $b_{ex}(t)$. That is, the rewinding pulse should have a K_{BS} equal to the negative of $b_{bs}(t)$'s K_{BS}, and scaled by $b_{ex}(t)$'s isodelay divided by the total duration of $b_{bs}(t)$.

Motion of the Magnetization Vector

With the full BSSE waveform defined, the trajectory of a magnetization vector $\vec{\mathbf{M}}$ during application of a BSSE RF pulse $b_{total}(t)$ can be described. Figures 4b and 4c show the motion of the normalized magnetization vector $\vec{\mathbf{M}}$ in a frame rotating at ω_{off} for spin isochromats in B_1^+ fields at 0.17 mT (in the stopband) and at 0.14 mT (in the passband), respectively, during application of the BSSE pulse of. During the first adiabatic sweep of the RF pulse, both magnetization vectors rotate down from equilibrium to an axis that is slightly tilted away from the x-y axis. At the end of the initial sweep, when $|b_{total}(t)| \approx |b_{bs}(t)|$ and $\Delta\omega_{rf}(t) \approx \omega_{off}$, $\vec{\mathbf{M}}$ is approximately colinear with the tilted effective field

$$\vec{\mathbf{B}}_{1,eff} = \left[\gamma B_1^+ \quad 0 \quad \omega_{off} \right] / \gamma$$

at which point the frequency-selective $b_{ex}(t)$ pulse begins. For the stopband isochromat of Fig. 4b this pulse is not resonant, but it is resonant with the isochromat of Fig. 4c and the magnetization is nutated by the component of $b_{ex}(t)$ perpendicular to $\vec{\mathbf{B}}_{1,eff}$ to the opposite side of the unit sphere. After $b_{ex}(t)$ is completed, the second adiabatic frequency sweep returns $\vec{\mathbf{M}}$ to being approximately colinear with the main magnetic field. The stopband isochromat in Fig. 4b is coaligned and approximately unperturbed from equilibrium, while the passband isochromat of Fig. 4c is successfully inverted. An video illustrating the magnetization motion is included as Supporting Information Video V1.

Compensating flip angle errors

The pulse design algorithm described above is based on the implicit approximation that the effect of applying $b_{bs}(t)$ is to produce a pure B_1^+-dependent resonance frequency shift. In reality, as illustrated in Fig. 4, $b_{bs}(t)$ rotates magnetization to precess in a plane that is slightly tilted from the x-y plane, at an angle $\tan^{-1}\left(\frac{\gamma B_1^+}{\omega_{off}}\right)$ from the z-axis. Ideally, $b_{ex}(t)$ would also be applied in this tilted plane, but it remains in the x-y plane, and the actual flip angle produced by $b_{ex}(t)$ will be slightly smaller than expected because its projection onto the tilted plane will be elliptical and smaller than its full amplitude. This results in a flip angle attenuation that increases as $\omega_{cent}/\omega_{off}$ becomes large. Similar effects have been previously observed in other dual-frequency RF applications (32, 33). Given the difficulty of describing and correcting this effect analytically, a normalized empirical correction is given herein for the amplitude of $A_{ex}(t)$ based on Bloch simulations of slice profiles across a wide range of ω_{cent} and ω_{off}. The model is shown in Fig. 5a, and the equations for the correction predicted by the model is provided in the Appendix. Deviations are generally small and require minimal correction for pulses where $\omega_{cent}/\omega_{off} < 1$ as suggested by the example profile correction shown in Fig. 5b. This comprises the majority of practical BSSE pulses. Pulses with ω_{cent} substantially larger than ω_{off} are in general encountered when designing a pulse to select a PBC at very large B_1^+ (which produces a large Bloch-Siegert shift and thus large ω_{cent} relative to ω_{off}), or when a very small ω_{off} is used, which is typically impractical due to the large out-of-band excitation produced.

Multiphoton Resonances

As discussed in the previous section, the simultaneous application of two off-resonance RF pulses in BSSE excitation leads to non-linear effects including small flip angle errors. A second effect is the appearance of subsidiary multiphoton resonances, in addition to the single-photon resonance. These are a consequence of the BSSE pulse's simultaneous irradiation of nuclei at two frequencies near (generally within 10's of kHz) but not at the Larmor frequency (24). While unwanted higher-order multiphoton resonances cannot be

corrected simply by adjusting the $b_{ex}(t)$ pulse's amplitude or frequency, their positions can be predicted analytically as follows and used to guide the pulse design.

The off-resonance frequencies of the two component pulses $b_{ex}(t)$ and $b_{bs}(t)$ are ω_{cent} and ω_{off}, with an average frequency of the two off-resonant pulses $\omega_{av} = \frac{1}{2}(\omega_{cent} + \omega_{off})$. Multiphoton resonances occur at frequencies $\omega_{0,N}$ for which the following is satisfied:

$$\left|\frac{\omega_1 - \omega_{av}}{\omega_{0,N} - \omega_{av}}\right| \approx \frac{1}{N}, \quad N = 1, 3, 5, \ldots,$$

where ω_1 is equivalently either ω_{off} or ω_{cent} (25). $N = 1$ corresponds to the single-photon resonance while $N = 3, 5, 7 \ldots$ correspond to multiphoton resonances. Arbitrarily taking $\omega_1 = \omega_{off}$, two solutions exist for $\omega_{0,N}$:

$$\omega_{0,N} \approx \omega_{av} \pm N(\omega_{off} - \omega_{av}) \tag{5}$$

In this application, because $\omega_{off} > 0$ will produce a negative frequency shift for all B_1^+, only $\omega_{0,N} < 0$ are of interest. These resonances are given by the solution $\omega_{0,N} \approx \omega_{av} + N(\omega_{off} - \omega_{av})$. To determine the locations of the multiphoton resonances on the B_1^+ axis, we can substitute Eq. 5 into Eq. 4, giving:

$$B_{1,mp}^+(N, \omega_{av}, \omega_{off}) \approx \frac{\omega_{off}}{\gamma}\sqrt{\left(1 - \frac{\omega_{av} + N(\omega_{off} - \omega_{av})}{\omega_{off}}\right)^2 - 1}, \quad N = 1, 3, 5, \ldots \tag{6}$$

Pulses with two combinations of ω_{off} and ω_{cent} but with the same PBC for the $N = 1$ excitation are shown in Figure 6a: the red pulses have ω_{off}=10 kHz and ω_{cent}=−1.655 kHz, and the black pulses have ω_{off}=7.5 kHz and ω_{cent}=−2.094 kHz. Figure 6b shows the distribution of multiphoton resonances across B_1^+ for the two ω_{off}. For both ω_{off}, the combination of RF frequencies place the $N = 1$ resonance at 0.14 mT. For the 90° and 180° pulses there is a small amount of excitation produced at the $N = 3$ resonance (maximum $|M_{xy}|/M_0 = 0.075$ for the excitation and maximum $M_z/M_0 = 0.918$ for the inversion), but excitation at $N > 3$ is below the stopband ripple level of the pulses. In the case of the pulse scaled up to produce a 720° flip, a greater number of multiphoton resonances can be appreciated. These simulated resonances shown in Figure 7b are at the approximate locations predicted by Equation 6; in the case of the black pulse (ω_{off} = 7.5 kHz), the resonances (aside from $N = 1$) are at $B_{1,mp}^+ = [0.14,\ 0.41,\ 0.65,\ 0.88,\ 1.11,\ 1.34]$ mT. In the case of the red pulse (ω_{off} = 10 kHz), the predicted locations of the $N = 1$ to 11 resonances shift up to $B_{1,mp}^+ = [0.14,\ 0.49,\ 0.79,\ 1.07,\ 1.35,\ 1.62]$ mT. Using a larger ω_{off} can shift multiphoton resonances upward in B_1^+ and out of the imaging bandwidth, although this decreases the Bloch-Siegert frequency gradient and thus requires longer pulse durations.

Methods

Simulations

Simulations were performed to demonstrate the effectiveness of SLR $B_N(\omega)$ ramp correction, to evaluate the pulses' suitability for refocusing in an RF gradient slice-selective CPMG pulse sequence, and to compare their performance to RFSE B_1^+-selective excitation pulses (16) in the presence of B_0 inhomogeneity and nonideal RF hardware. All simulations were performed using a hard pulse approximation-based Bloch simulator (27) in SigPy.RF (35) with 1 μs dwell time. All BSSE and RFSE pulses were designed using SigPy.RF pulse design functions. Code for BSSE pulse design is available at: https://github.com/jonbmartin/sigpy-rf.

Profile Ramp Correction

Simulations were performed to verify the ability of the BSSE ramp correction algorithm to correct passband distortions caused by varying B_1^+. A 30° small-tip pulse, a 90° excitation pulse, and a 180° inversion pulse were constructed and their magnetization profiles were simulated across B_1^+. For all three pulses, PBC = 0.14 mT, PBW = 0.06 mT, $T_{ex}B = 8$, $d_1^e = d_2^e = 0.01$, $\omega_{off} = 7.5$ kHz; these parameters were chosen to create a profile in which uncorrected distortions were clearly visible. In profiles with smaller $T_{ex}B$ or PBW, the distortion is not easily observable. The small-tip and 90° excitation pulses were designed using the analytic $B_N(\omega)$ ramp correction. In the inversion case, an uncorrected BSSE inversion pulse was designed to meet the profile parameters specified above as well as possible. This pulse was used as the initializer for an iterative gradient descent refinement to eliminate distortions. The following general unconstrained problem was solved:

$$\min_{\boldsymbol{b}_{total}} \sum_{i=0}^{N_b-1} w_i \left| \boldsymbol{M}_z\left(\boldsymbol{b}_{total}, B_{1,i}^+\right) - \boldsymbol{M}_{z,d}\left(B_{1,i}^+\right) \right|^2, \tag{7}$$

where $\left\{ M_z\left(\boldsymbol{b}_{total}, B_{1,i}^+\right) \right\}_{i=0}^{N_b-1}$ is the Bloch-simulated M_z Profile of the BSSE pulse vector $\boldsymbol{b}_{total}$ across transmit field strengths $\left\{B_{1,i}^+\right\}_{i=0}^{N_b-1}$, and $\left\{ M_{z,d}\left(B_1^+\right) \right\}_{i=0}^{N_b-1}$ is the desired inversion profile across the same B_1^+ range. The $\{w_i\}$ are error weights used to specify the transition regions of the profile as 'don't care' regions for the optimization. The gradient of the loss was calculated across a grid of 250 points in B_1^+ from 0 to 0.25 mT using an automatic differentiation function from the JAX software toolbox (36). Gradient descent steps were taken to minimize this loss, with a fixed step size of 1e−4. Iterations were performed until convergence, defined as a difference in loss between iterations of less than 1%.

Off-Resonance Simulation

Four BSSE pulses and four RFSE pulses were designed, with ω_{off} of the BSSE pulses set to give the pulses the same duration as the RFSE pulses. The 'base' pulse for both pulse classes

was a 6.27 ms $T_{ex}B = 4$ pulse at 90° flip angle, centered at PBC = 0.4 mT with PBW = 0.03 mT and M_{xy} passband and stopband maximum errors of $\delta_1^e = \delta_2^e = 0.01$. The other three pulses each had one parameter changed from the base pulse (Pulse 1): Pulse 2 had its' PBW doubled to 0.06 mT (decreasing the duration to 3.14 ms), Pulse 3 had its' time bandwidth product doubled to 8 (increasing the duration to 12.53 ms), and Pulse 4 had its' PBC shifted to 0.15 mT (keeping the duration of the pulses fixed at 6.27 ms). ω_{off} for the four BSSE pulses were set to 16.370 kHz, 9.485 kHz, 19.250 kHz, and 8.170 kHz, respectively, to match RFSE pulse durations. Magnetization was simulated over a B_1^+ range of 0–0.5 mT and an off-resonance range of 0–1 kHz.

RF Amplifier Droop Simulation

A weakness of RFSE B_1^+-selective pulses is their requirement that the pulse AM envelope be carefully balanced (16), since the pulses operate by spinning magnetization in the *y*-*z* plane while tipping magnetization in the passband towards *x*, and any errors in the envelope will result in large undesired excitation in *y*. This is a challenging demand for many RF amplifiers. RF amplifier droop was simulated for both a BSSE and an RFSE pulse to compare their robustness. Both pulses were designed with PBC=0.14 mT, PBW=0.03 mT, $T_{ex}B = 4$, 45° flip angle, and $\delta_1^e = \delta_2^e = 0.01$. ω_{off} of the BSSE pulse was set to 7.608 kHz to match the durations of the two pulses (6.22 ms). Droops of −0.5 dB and −1.5 dB in the relative pulse amplitudes across the total duration were simulated (Figures 8a, 8c).

CPMG Sequence Simulation

A multi-echo spin echo pulse sequence was constructed using BSSE excitation and refocusing pulses. The same BSSE pulse parameters were used as in the previous experiment (PBC = 0.14 mT, PBW = 0.03 mT, $T_{ex}B = 4$, ω_{off}=7.5 kHz, T = 6.22 ms) to design a 90° excitation pulse and a 180° refocusing pulse. The BSSE refocusing pulse was iteratively refined to eliminate any ramped B_1^+ distortion.

The $b_{bs}(t)$ design algorithm was used to generate a pair of RF pulses serving as B_1^+ phase pre- and rewinder gradients. These pulses were given an equal-magnitude/opposite-signed ω_{off} as the BSSE pulse to produce a shift in resonant frequency opposite that of the refocusing pulse, with $|K_{BS}|$ half that of the refocusing pulse (32.2 vs 16.1 rad^2/G). The 90° BSSE excitation pulse was applied along the *x*-axis and was followed by eight refocusing pulses applied along the *y*-axis for an echo train length of 8, with TE = 2τ = 33 ms. The RF pulse sequence diagram is shown in Figure 9a. The pulses were simulated across a B_1^+ range of 0 to 0.3 mT and a range of frequency offsets between −200 and 200 Hz, with $T_1 = T_2 = \infty$.

Experiments

Phantom experiments were performed to verify the magnetization profiles produced by BSSE pulses. A base BSSE pulse with flip angle 90°, PBC = 0.14 mT, PBW = 0.03 mT, ω_{off} = 7.5 kHz, $T_{ex}B = 4$, and total duration T = 6.22 ms was designed. Three copies of

the pulse were created in which a single parameter was varied: passband center (0.14 mT → 0.11 mT), flip angle (90° → 45°), and time-bandwidth product (4 → 1.5). The pulses were deployed on a 47.5 mT permanent magnet (Fig 10a) (Sigwa MRI, Boston, MA, USA) and image data were acquired using a Tecmag Redstone MRI Console (Tecmag, Houston, Texas, USA). The system used a 1 μs transmit dwell time and amplitude/phase tables for RF waveform definition. A 2 kW BT02000-AlphaS Tomco RF power amplifer (Tomco Rechnologies, Stepney, Australia) was used to drive a 20-turn variable-pitch solenoid RF T/R coil producing a linearly decreasing B_1^+ gradient (Fig 10b). A 50 mL 1 mM CuSO4 vial phantom with 30 mm diameter and 115mm length was imaged using a 3D gradient-recalled echo pulse sequence (TR/TE = 27/425 ms, dx/dy/dz = 2.0/3.5/3.5 mm, matrix size = 128×49×3, 5 signal averages), where the BSSE pulses were used for excitation. Phase variation produced across the excitaton profile by the BSSE excitation pulse was not rewound in this pulse sequence. Conventional B_0 gradients were used for image spatial encoding. B_1^+ mapping was also performed using the BS shift method (18) with the same 3D gradient-recalled echo sequence but with the addition of a hard pulse excitation. The 6.22 ms, ω_{off}=7.5kHz component of the BSSE pulse was kept as the B_1^+-dependent phase shift-generating pulse (K_{BS} = 32.2 rad^2/G) for B_1^+ mapping, producing no excitation without the addition of the $b_{ex}(t)$ component pulse. To process the images, a mask was created by thresholding a 90° hard pulse GRE acquisition with the same matrix size and resolution to 20% of the maximum signal intensity. This mask was applied to the phase images of the B_1^+-mapping sequence and magnitudes of the BSSE-excitation images. The B_1^+ mapping phase image was unwrapped along the coil's gradient dimension, and background phase was subtracted out using a reference scan without a BS shift pulse. B_1^+ strength was then calculated using the K_{BS} of the off-resonant pulse. The BSSE excitation images were divided by the B_1^+ map to remove the receive sensitivity of the T/R coil, since $\left|B_1^+\right| \sim \left|B_1^-\right|$ at this low frequency.

Results

Ramp Correction Simulation

Figures 2b–d shows the improved small-tip excitation, 90° excitation, and inversions with ramp correction. The small-tip excitation had a substantial ramp across B_1^+ when uncorrected which was flattened by the analytic correction, with differences between normalized $\left|M_{xy}\right|/M_0$ at passband edges reduced from 0.0893 in the uncorrected case to less than 0.001 in the corrected case. The 90° excitation also had substantially reduced distortion in the passband, particularly on the rising edge of the profile. Iterative optimization of the inversion pulse reached convergence after 37 gradient descent iterations. The final optimized pulse produced a substantially improved magnetization profile which met the desired ripple levels $\left(d_1^e = d_2^e = 0.01\right)$ and transition width. The substantial ripple produced by over-flipping on the falling edge of the profile was eliminated, and the broad transition on the rising edge of the profile was sharpened.

Off-Resonance Simulations

The results of the off-resonance simulation are shown in Fig. 7. All RFSE pulses produced a triangular pattern of erroneous excitation where the effective size of the off-resonance field was large compared to the B_1^+ field. This effect is absent from the BSSE pulse profiles. At the same time, all four BSSE pulses show a small bulk downward shift in the excitation profile with increasing off-resonance, similar to a conventional B_0 gradient-selective excitation pulse. For the four BSSE pulses shown in Figures 8a–d, the shift was −0.033 mT/kHz, −0.019 mT/kHz, −0.038 mT/kHz, and −0.036 mT/kHz. As expected, the slope of the shift correlated with pulse duration: the pulse with the shortest duration (3.14 ms) also had the smallest bulk shift (−0.019 mT/kHz). A faint $N = 3$ multiphoton resonance is visible in Figure 8d at approximately 0.45 mT. The $N = 3$ resonance also exhibited a shift downward in B_1^+ with off-resonance.

RF Amplifier Droop Simulation

The effect of RF amplifier droop on the magnetization profile is shown in Figures 8b and 8d. For the RFSE pulse, pulse droop significantly distorted the excitation profile. −0.5 dB of droop reduced the transverse magnetization by approximately 13%; −1.5 dB of droop completely degraded the magnetization profile. In the case of the BSSE pulse, however, the same droop produced minimal distortion, manifesting primarily as a small shift in the magnetization profile. This shift was approximately 0.004 mT (13% of slice width) in the case of −0.5 dB of droop and 0.013 mT (43% of slice width) in the case of the −1.5 dB droop.

CPMG Simulation

Figures 9b and 9c show the results of the multi-echo spin echo sequence simulation. The refocusing profile in Fig. 9b shows close to full refocusing efficiency within the pulses' 0.03 mT-wide passband. This is supported by Fig. 9c, which shows the signal integrated across off-resonance at a location in the passband (0.14 mT) and the stopband (0.17 mT). In the passband evenly spaced echoes are formed, with near-identical signal amplitude produced at each echo. In the stopband, no appreciable signal was produced at the echo times.

Experimental Results

Figures 10c–f show the measured experimental profiles for the pulses played out in the experiment in the central slice of the 3D acquisition. Figure 10g shows the corresponding B_1^+ map from the same slice. 1D profiles of the simulated (Fig 10h) and experimental (Fig 10i) are shown as well. In the experimental case these were generated by averaging across the z dimension of the profile. For the two-flip angle (90° to 45°) experiment, a decrease in signal intensity was observed consistent with the expected 30% decrease based on the nominal flip angles. The ratio of the signals from the 45° and 90° excitations between the passband edges was 0.705 in simulation and 0.627 in the experiment. In the case of decreasing $T_{ex}B$ from 4 to 1.5, the $T_{ex}B = 1.5$ profile had a wider transition width resulting from the decrease in selectivity. The ratio of the full width at half-maximum of the profiles from the $T_{ex}B = 1.5$ excitation and the $T_{ex}B = 4$ excitation was 1.29 in simulation and 1.21 in the experiment,

showing close agreement. The pulse with PBC shifted to 0.11 mT produced a magnetization profile centered at the intended locations, and the transition bands of the pulses intersected at approximately 0.125 mT, where each profile was expected to reach its half-maximum.

The phase produced by the BSSE excitation pulses across the magnetization profile is shown in Supporting Information Figure S1. For all four of the BSSE pulses that were examined, the phase of the spins increased in an approximately linear manner across the magnetization profile, with uniform spacing between successive phase wraps over the linearly increasing B_1^+ transmit field.

Discussion

A class of excitation pulses that apply the Bloch-Siegert shift for the purpose of selective excitation was introduced. Although the Bloch-Siegert shift has been widely used in MRI for B_1^+ mapping (18, 30) and in NMR for the calibration of decoupling field power (20, 37), to our knowledge the present work represents its first use to localize selective excitation. Simulation results showed that the pulses are robust against system imperfections and can be used in pulse sequences requiring phase control, making them a viable choice for a wide range of pulse sequences. Overall, BSSE pulses enable the replacement of one axis of B_0 gradient encoding with B_1^+ gradient encoding in an imaging system. Most RF encoding systems experimentally implemented thus far including the imaging experiments performed in this work have relied on at least one axis of B_0 encoding for 3D imaging (5, 6), and further development is needed to achieve fully RF-encoded 3D imaging. More immediately, BSSE selective excitation could be combined with other pulsed B_0 gradient-free imaging systems, such as systems with built-in B_0 field inhomogeneities (39–41).

As in the RFSE design algorithm of (16), the proposed BSSE pulse design method is based on the Shinnar-Le Roux algorithm, giving BSSE pulses the same advantage in speed of design and ability to predict and trade off design parameters. However the proposed method also has a number of advantages over RFSE pulses, including the ability to refocus magnetization for spin-echo based pulse sequences, and reduced out-of-band excitation in response to B_0 inhomogeneity. RFSE pulses can also be challenging to implement experimentally because they place strict requirements on the integrated area of the RF envelope, which must be accurately balanced between pulse segments to prevent large distortions of the magnetization profile. In this work BSSE pulses were shown to be more tolerant of moderate amplifier errors in the amplitude of the RF pulse, such as amplifier droop, which led primarily to relatively benign slice shifts which could be mostly corrected by transmit gain adjustment.

BSSE pulse designers should keep several practical considerations in mind. First, the BSSE pulses demonstrated here had relatively longer durations than conventional B_0 gradient-selective excitations (several ms versus a few ms). For a fixed $b_{ex}(t)$ time-bandwidth product $T_{ex}B$, BSSE pulse length is principally determined by two factors: the B_1^+ gradient strength for a given $b_{bs}(t)$ amplitude and ω_{off}, the central constant frequency offset of $b_{bs}(t)$. These variables determine the magnitude of the Bloch-Siegert frequency gradient produced by

$b_{bs}(t)$, which in turn sets the duration of the full BSSE pulse. If the Bloch-Siegert spatial frequency gradient were of the same magnitude as a B_0 spatial frequency gradient, a BSSE pulse would have approximately the same duration as an equivalent conventional B_0 gradient selective excitation pulse. For example, to create a frequency gradient of 1 MHz/m (produced by a B_0 gradient of approximately 23.5 mT/m) using the Bloch-Siegert shift, using the ω_{off}=7.5kHz value used throughout this work, a B_1^+ gradient of approximately the same strength, 23.5 mT/m, would be required. Though a much weaker B_1^+ gradient of ~2 mT/m was used here experimentally, this stronger gradient is not difficult to achieve in practice (5, 7). In general, ω_{off} should be minimized to maximize the Bloch-Siegert frequency gradient. However, excessive reduction of the frequency offset can produce out-of band excitation (Figure 3b, at ω_{off}=2.5kHz) or move multiphoton resonances closer in B_1^+ to the single-photon resonance (Figure 6) and potentially into the FOV. Although their rapid dropoff in amplitude with N makes their use for imaging challenging, it may be possible to use BSSE pulses for multiband multiphoton excitation in implementations similar to those previously described (26). However in general ω_{off} should be increased to move multiphoton resonances outside the FOV.

The RF power and consequently the specific absorption rate (SAR) contribution of BSSE pulses is increased compared to an equivalent B_0 gradient-selective excitation by the addition of the large, near-constant AM waveform of the off-resonant $b_{bs}(t)$ pulse to the on-resonant $b_{ex}(t)$ pulse. Since the pulses are well-separated in frequency, the power increase compared to a conventional pulse is approximately equal to the power of the $b_{bs}(t)$ component. For example, for the 6.22 ms BSSE pulse shown in Figure 1, operating at 47.5 mT, the integrated power of $b_{ex}(t)$ normalized by that of the full $b_{total}(t)$ was 4×10^{-4} (a.u.), and the integrated power of $b_{bs}(t)$ normalized by that of $b_{total}(t)$ was 0.9996 (a.u.). Nearly all power is contributed by the $b_{bs}(t)$ pulse. At the same time, SAR is much less a concern in low-field MRI such as the 47.5 mT imager used in this work (42).

Like conventional B_0 gradient-selective excitations, as demonstrated experimentally, BSSE pulses leave a phase gradient across the excited slice that should be refocused if subsequent imaging will not resolve the slice dimension. Refocusing can be achieved with a rewinding off-resonant $b_{bs}(t)$ pulse, to cancel phase accrued during the pulse's isodelay. At the same time, like conventional B_0 gradient-selective excitations, there are many situations where this is not necessary, including when using the pulses for saturation, inversion, or for slab selection in 3D imaging sequences. When used for slice-selective excitation, using a minimum-phase $b_{ex}(t)$ pulse shape with a small isodelay would also reduce or eliminate the need for a rewinder. When using BSSE pulses for balanced or spin echo pulse sequences, RF pre- and rewinders may be inserted into the pulse sequence.

The experimental setup in this work used a single gradient coil for transmit and receive which is nonideal in practice, since although profiles with uniform flip were excited across the slice, the coil's nonuniform receive sensitivity would result in spatially varying SNR. To alleviate this, the gradient transmit coil could be paired with a saddle receive coil with uniform receive sensitivity, which has been demonstrated on the 47.5 mT system described here (43).

The pulse design algorithm described here could be extended in numerous ways. Applying the VERSE algorithm (44) may allow the frequency-selective excitation pulse to extend onto the time-varying portion of the Bloch-Siegert shift inducing pulse, to shorten overall pulse duration. Additionally, BSSE pulse designs may benefit from joint gradient-based optimization of the two component pulses, in analogy to previously demonstrated joint optimization of RF and gradient waveforms (45). Further optimizing the waveforms this way could be used to, e.g., reduce multiphoton effects, decrease pulse duration, produce uniform excitation across a broad range of B_1^+, or constrain the pulses to have a flat amplitude so they can be more easily generated by current-mode amplifiers(46). Finally, the pulses could be extended to produce Hadamard or other multiband excitations, by designing the excitation pulse $b_{ex}(t)$ using multiband pulse designers developed for B_0 gradient-based selective excitation (47–49).

Conclusion

In this work, we presented a novel class of pulses for B_1^+-selective excitation which localize excitation using frequency gradients produced by the Bloch-Siegert shift. Simulations demonstrate that these pulses produce magnetization profiles of excellent quality with phase control, and that the pulses are robust against off-resonance. Experimental results on an ultra-low-field 47.5 mT verified the design algorithm's ability to control magnetization profile parameters. BSSE pulses may help enable new methods of B_0-gradient-free acquisition and novel imaging approaches.

Supplementary Material

Refer to Web version on PubMed Central for supplementary material.

Acknowledgments

This work was supported by NIH grants R01 EB 030414 and R01 EB 016695. The authors would like to thank Benjamin Hardy for many helpful conversations about this work.

Appendix

The models used to correct for flip angle inaccuracy is as follows. The observed flip angle attenuation was fit by a biexponential model, using MATLAB's fit() function. This attenuation model is:

$$\Gamma(x) = 0.335e^{-1.116x} + 0.678e^{-0.028x},$$

where $x = \omega_{cent}/\omega_{off}$. The correction is applied by accounting for $\Gamma(x)$ in the flip angle relation of Eq. 3:

$$\theta = \gamma \Delta_t \Gamma(x) B_1^+(\omega_{cent}) \sum_{i=0}^{N-1} A_{ex}(t_i),$$

The goodness-of-fit of this model was $R^2 = 0.9899$.

References

[1]. Bernstein MA, Zhou XJ, Polzin JA, King KF, Ganin A, Pelc NJ, Glover GH. Concomitant gradient terms in phase contrast MR: Analysis and correction. Magnetic Resonance in Medicine 1998; 39(2):300–308. [PubMed: 9469714]

[2]. Spees WM, Buhl N, Sun P, Ackerman JJ, Neil JJ, Garbow JR. Quantification and compensation of eddy-current-induced magnetic-field gradients. Journal of Magnetic Resonance 2011; 212(1):116–123. [PubMed: 21764614]

[3]. Hoult DI. Rotating frame zeugmatography. Journal of Magnetic Resonance 1979; 33(1):183–197.

[4]. Sharp JC, King SB. MRI using radiofrequency magnetic field phase gradients. Magnetic Resonance in Medicine 2010; 63(1):151–161. [PubMed: 19918899]

[5]. Kartäusch R, Driessle T, Kampf T, BasseLüsebrink TC, Hoelscher UC, Jakob PM, Fidler F, Helluy X. Spatial phase encoding exploiting the Bloch–Siegert shift effect. Magnetic Resonance Materials in Physics, Biology and Medicine 2014; 27:363–371.

[6]. Torres E, Froelich T, Wang P, DelaBarre L, Mullen M, Adriany G, Pizetta DC, Martins MJ, Vidoto ELG, Tannús A, Garwood M. B1-gradient–based MRI using frequency-modulated Rabi-encoded echoes. Magnetic Resonance in Medicine 2021; 87(2)674–685:. [PubMed: 34498768]

[7]. Canet D Radiofrequency field gradient experiments. Progress in Nuclear Magnetic Resonance Spectroscopy 1997; 30(1–2):101–135.

[8]. Tycko R, Pines A. Spatial localization of NMR signals by narrowband inversion. Journal of Magnetic Resonance 1984; 60(1):156–160.

[9]. Shaka AJ, Freeman R. Spatially selective radiofrequency pulses. Journal of Magnetic Resonance 1984; 59(1):169–176.

[10]. Garwood M Localized MRS Employing Radiofrequency Field (B1) Gradients. eMagRes 2016; 5(1):1015–1025.

[11]. Bendall M, Gordon R. Depth and refocusing pulses designed for multipulse NMR with surface coils. Journal of Magnetic Resonance 1983; 53(3):365–385.

[12]. Hoult DI. NMR imaging. Rotating frame selective pulses. Journal of Magnetic Resonance 1980; 38(1):369–374.

[13]. Karczmar GS, Lawry TJ, Weiner MW, Matson GB. Shaped pulses for slice selection in the rotating frame-A study using computer simulations. Journal of Magnetic Resonance 1988; 76(1):41–53.

[14]. Maffei P, Elbayed K, Brondeau J, Canet D. Slice selection in NMR imaging by use of the B1 gradient along the axial direction of a saddle-shaped coil. Journal of Magnetic Resonance 1991; 95(2):382–386.

[15]. Hedges LK, Hoult DI. The techniques of rotating frame selective excitation and some experimental results. Journal of Magnetic Resonance 1988; 79(3):391–403.

16. [] Grissom WA, Cao Z, Does MD. B_1^+-selective excitation pulse design using the Shinnar-Le Roux algorithm. Journal of Magnetic Resonance 2014; 242(1):189–196. [PubMed: 24674887]

[17]. Bloch F, Siegert A. Magnetic Resonance for Nonrotating Fields. Physical Review 1940; 57(6):522.

[18]. Sacolick LI, Wiesinger F, Hancu I, Vogel MW. B1 mapping by Bloch-Siegert shift. Magnetic Resonance in Medicine 2010; 63(5):1315–1322. [PubMed: 20432302]

[19]. Hosur RV, Ernst RR, Wothrich K. A simple two-dimensional measurement of the decoupler power during continuous homonuclear irradiation for the correction of Bloch-Siegert shifts. Journal of Magnetic Resonance 1983; 54(1):142–145.

[20]. Hung I, Gor'kov P, Gan Z. Using the heteronuclear Bloch-Siegert shift of protons for B1 calibration of insensitive nuclei not present in the sample. Journal of Magnetic Resonance 2020; 310(1):1–5.

[21]. Zhipeng C, Chekmenev EY, Grissom WA. Frequency encoding by Bloch-Siegert shift. In: Proc. Intl. Soc. Mag. Reson. Med, Milan, Italy p. 4220 (2014).

[22]. Wan Y, Qiu M, Galiana G, Constable R. Phase Encoding with Bloch-Siegert effect using Parallel Transmit. In: Proc. Intl. Soc. Mag. Reson. Med, Honolulu, USA p. 1498 (2017).

[23]. Martin J, Vaughn C, Griswold MA, Grissom WA. Bloch-Siegert $|B_1^+|$-Selective Excitation Pulses. In: Proc. Intl. Soc. Mag. Reson. Med, Virtual p. 3337 (2021).

[24]. Zur Y, Levitt MH, Vega S. Multiphoton NMR spectroscopy on a spin system with I=1/2. The Journal of Chemical Physics 1983; 78(9):5293.

[25]. Krauss EM, Vega S. Four-field excitation of multiphoton NMR resonances in spin I=1/2. Physical Review A 1986; 34(1):333.

[26]. Han V, Liu C. Multiphoton magnetic resonance in imaging: A classical description and implementation. Magnetic Resonance in Medicine 2020; 84(3):1184–1197. [PubMed: 32022369]

[27]. Pauly J, Nishimura D, Macovski A, Roux PL. Parameter Relations for the Shinnar-Le Roux Selective Excitation Pulse Design Algorithm. IEEE Transactions on Medical Imaging 1991; 10(1):53–65. [PubMed: 18222800]

[28]. Ramsey NF. Resonance transitions induced by perturbations at two or more different frequencies. Physical Review 1955; 100(4):1191–1194.

[29]. Garwood M, DelaBarre L. The Return of the Frequency Sweep: Designing Adiabatic Pulses for Contemporary NMR. Journal of Magnetic Resonance 2001; 153(2):155–177. [PubMed: 11740891]

[30]. Khalighi MM, Rutt BK, Kerr AB. Adiabatic RF Pulse Design for Bloch-Siegert Mapping. Magnetic Resonance in Medicine 2013; 70:829–835. [PubMed: 23041985]

[31]. Hannaford P, Pegg DT, Series GW. Analytical expressions for the Bloch-Siegert shift. Journal of Physics B: Atomic and Molecular Physics 1973; 6:L222–L225.

[32]. Mccoy MA, Mueller L. Selective Decoupling. Journal of Magnetic Resonance, Series A 1993; 101(2):122–130.

[33]. Steffen M, Vandersypen LMK, Chuang IL. Simultaneous Soft Pulses Applied at Nearby Frequencies. Journal of Magnetic Resonance 2000; 146:369–374. [PubMed: 11001853]

[34]. Vega S Multiple-quantum cross-polarization NMR on spin systems with I=1/2 and S=3/2 in solids. Physical Review A 1981; 23:3152.

[35]. Martin J, Ong F, Ma J, Tamir J, Lustig M, Grissom W. SigPy.RF: Comprehensive Open-Source RF Pulse Design Tools for Reproducible Research. In: Proc. Intl. Soc. Mag. Reson. Med 28th Annual Meeting, Virtual p. 1045, (2020).

[36]. Frostig J, Johnson MJ, Leary C. Compiling machine learning programs via high-level tracing, In: SYSML, Stanford, USA (2018).

[37]. Claridge TD. High-Resolution NMR Techniques in Organic Chemistry 3rd Ed. Cambridge, MA:Elsevier 2016;1–541.

[38]. Duan Q, Gelderen Pv, Duyn J. Improved Bloch-Siegert Based B1 Mapping by Reducing Off-Resonance Shift. NMR in Biomedicine 2013; 26(9):1070. [PubMed: 23355474]

[39]. Stockmann J, Cooley C, Guerin B, Rosen M, Wald L. Transmit Array Spatial Encoding (TRASE) using broadband WURST pulses for RF spatial encoding in inhomogeneous B0 fields. Journal of Magnetic Resonance 2016; 268:36–48. [PubMed: 27155906]

[40]. Cooley C, Stockmann J, Armstrong B, Sarracanie M, Lev M, Rosen M, Wald L. Two-dimensional imaging in a lightweight portable MRI scanner without gradient coils. Magnetic Resonance in Medicine 2015; 73(2):872–883. [PubMed: 24668520]

[41]. Sarty G Cyclic generalized projection MRI. Magnetic Resonance Imaging 2015; 33(3):304–311. [PubMed: 25532468]

[42]. Van Speybroeck CDE, O'Reilly T, Teeuwisse W, Arnold PM, Webb AG. Characterization of displacement forces and image artifacts in the presence of passive medical implants in low-field (<100 mT) permanent magnet-based MRI systems, and comparisons with clinical MRI systems. Physica Medica 2021; 84:116–124. [PubMed: 33894581]

[43]. Srinivas S, Vaughn C, Martin J, Grissom W. EMI-Suppressed Gradient-Free Phase-Encoded Imaging at 47.5mT Using an Optimized Square-Root Solenoid with Bucking Coil for Encoding and a Nested Saddle Coil for Imaging. In: Proc. Intl. Soc. Mag. Reson. Med, London, UK (2022).

[44]. Hargreaves B, Cunningham C, Nishimura D, Conolly S. Variable-rate selective excitation for rapid MRI sequences. Magnetic Resonance in Medicine 2004; 52:590–597. [PubMed: 15334579]

[45]. Luo T, Noll DC, Fessler JA, Nielsen JF. Joint Design of RF and gradient waveforms via auto-differentiation for 3D tailored excitation in MRI. IEEE TMI 2021; 40:3305–3314.

[46]. Bolding R, Vaughn C, BladesThomas C, Grissom W, Griswold M. Low-cost Modular RFPA Platform for Gradient-Free Quantitative Imaging. In: Proc. Intl. Soc. Mag. Reson. Med, London, UK (2022).

[47]. Cunningham CH, Wood ML. Method for Improved Multiband Excitation Profiles Using the Shinnar-Le Roux Transform. Magnetic Resonance in Medicine 1999; 42:577. [PubMed: 10467303]

[48]. Sharma A, Lustig M, Grissom WA. Root-flipped multiband refocusing pulses. Magnetic Resonance in Medicine 2016; 75(1):227–237. [PubMed: 25704154]

[49]. Ma J, Witzel T, Grissom WA, Setsompop K. Minimum peak power root-flipped gSlider-SMS RF pulses for high-resolution in vivo diffusion imaging. In: Proc. Intl. Soc. Mag. Reson. Med, Honolulu, USA p. 0523 (2017).

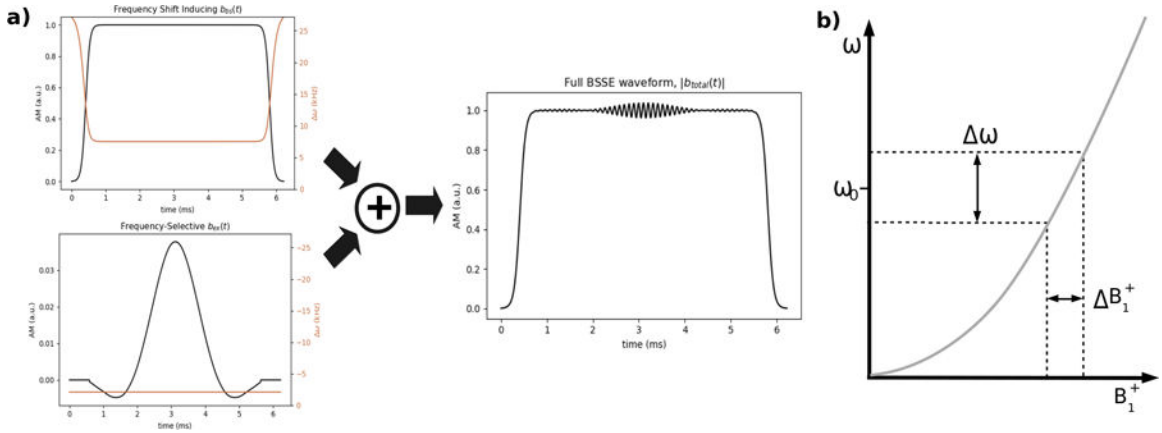

Figure 1.

a) Construction of a BSSE RF pulse. The Bloch-Siegert shift producing pulse $b_{bs}(t)$ (top left) and slice-selective pulse $b_{ex}(t)$ (bottom left) are designed independently and summed into the full BSSE waveform $b_{total}(t)$. $b_{bs}(t)$ has Fermi AM (black) and adiabatic frequency sweeps towards and away from a constant frequency offset ω_{off} (orange). $b_{ex}(t)$ has SLR-designed AM (black) and a constant frequency offset (orange). The amplitude of the $b_{bs}(t)$ waveform is generally much larger than that of the $b_{ex}(t)$ waveform; in $|b_{total}(t)|$, $b_{ex}(t)$ is visible as a small ripple in the plateau of the Fermi waveform. b) Bloch-Siegert shift-localized slice selection, in which an off-resonant RF pulse produces an approximately quadratic variation in resonant frequencies across field strengths B_1^+. When paired with a frequency-selective excitation pulse, this results in the excitation of spins across a range ΔB_1^+, which can be mapped to space using an amplitude gradient transmit coil.

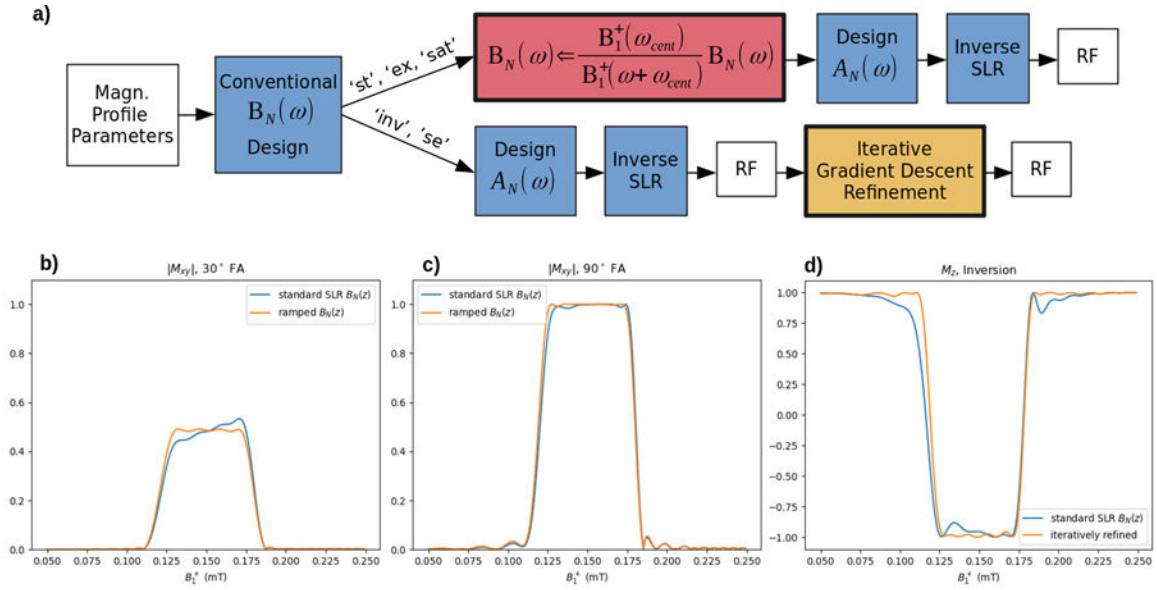

Figure 2.

a) SLR design algorithm to compensate for a sloped excitation profile across B_1^+. In the case of small-tip ('st') or 90° ('ex', 'sat') excitation, a pointwise scaling of the $B_N(\omega)$ profile is sufficient. For an inversion ('inv') or refocusing ('se') pulse, iterative refinement is required. b) Uncorrected and corrected 30°, PBC = 0.15 mT, PBW = 0.06 mT, $T_{ex}B$ = 8 excitation. c) Uncorrected and corrected 90° excitation. d) Uncorrected and corrected inversion profile after autodifferentiated gradient descent optimization of the pulse with respect to its magnetization profile, Iterative refinement corrected the highly distorted transition bands of the profile.

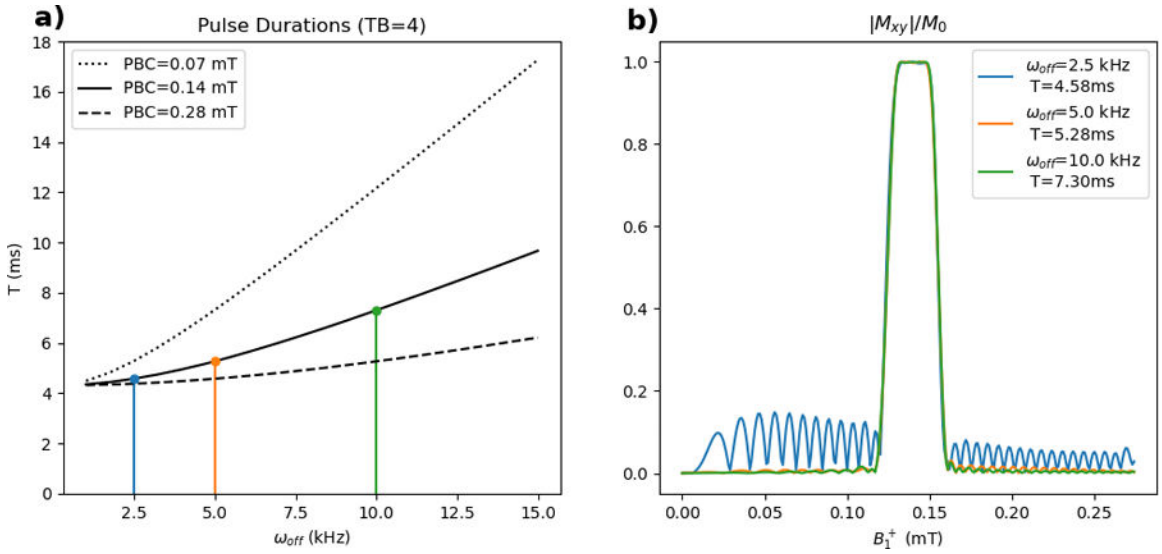

Figure 3.

a) Variation in BSSE pulse duration with ω_{off} and PBC in B_1^+. Pulse duration increases with increasing ω_{off} and decreases with increasing B_1^+ PBC. The magnetization profiles of pulses designed at the three points of interest are plotted in (b). b) Magnetization profiles of BSSE pulses with PBC=0.14mT. Out-of band excitation can be large if ω_{off} is set too small: a pulse with ω_{off} = 2.5 kHz produces a substantial amount of out-of-band excitation, which is reduced to within design specifications when $\omega_{off} \rightarrow$ 5.0 kHz. Further increasing ω_{off} to 10.0 kHz produced only marginal improvement.

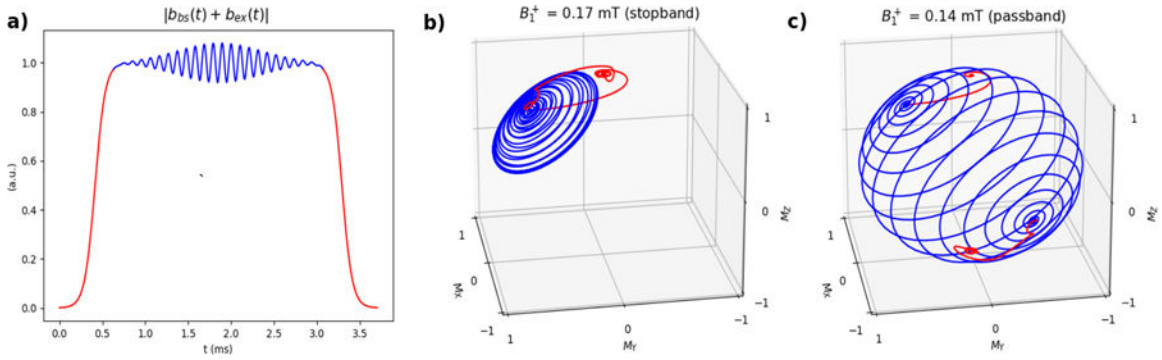

Figure 4.

a) Magnitude of a $T = 3.7$ ms BSSE inversion pulse. The pulse is colored red during the adiabatic frequency sweeps when $b_{ex}(t) = 0$, and blue during the constant portion of $b_{bs}(t)$ when $b_{ex}(t) \neq 0$. b) Motion of the net magnetization vector in the ω_{off} rotating frame for a stopband isochromat. Simulation timestep was 4 μs. At the end of the pulse, magnetization is essentially unperturbed. c) Motion of the net magnetization vector in the ω_{off} rotating frame for a passband isochromat. At the end of the pulse, magnetization is successfully inverted.

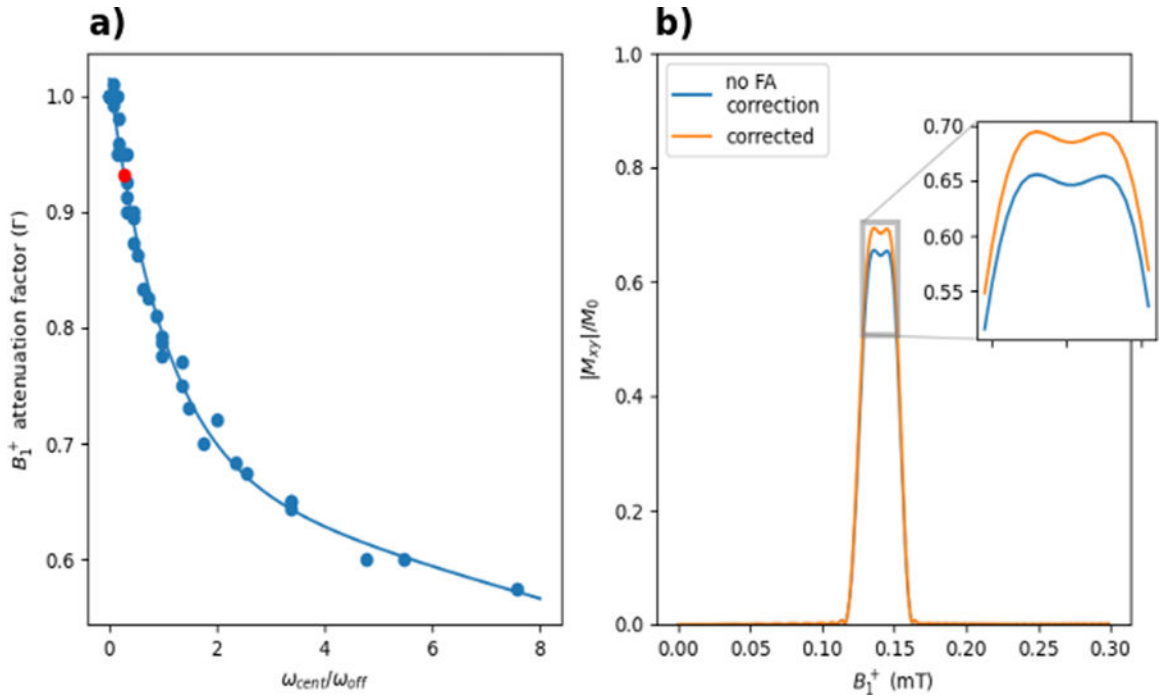

Figure 5.

a) Flip angle attenuation factor versus $\omega_{cent}/\omega_{off}$. Data points are empirical correction factors found through simulation, with an exponential fit to the data shown as a continuous line. The red dot indicates the parameters of the pulse simulated in (b). b) Excited slice profile of a PBC =0.14 mT, PBW = 0.03 mT, 45°, ω_{off} =7.5 kHz pulse with and without the empirical FA correction. For this pulse, $\omega_{cent}/\omega_{off}$ = 0.279, which the model predicts will result in a flip angle attenuation of 6.9% if uncorrected. Applying the correction improves the effective flip angle of the pulse, bringing it closer to the anticipated $|M_{xy}|/M_0$ = 0.7

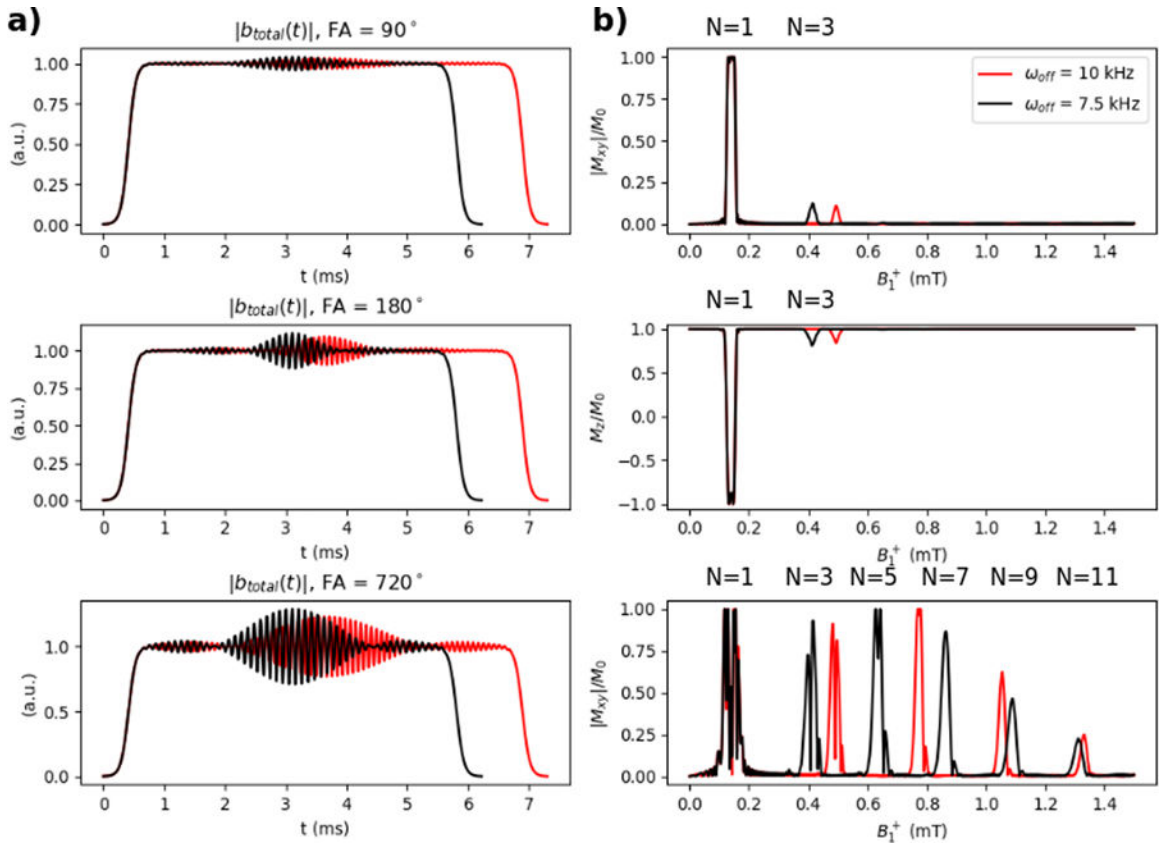

Figure 6.

a) Magnitudes of 90°, 180°, and 720° BSSE pulses with ω_{off} = 7.5 kHz (black) and ω_{off} = 15.0 kHz (red). b) The corresponding simulated magnetization profiles. Multiphoton resonances are visible at the locations in B_1^+ predicted by Equation 6. Increasing ω_{off} shifts resonances $N \geq 3$ upward in B_1^+.

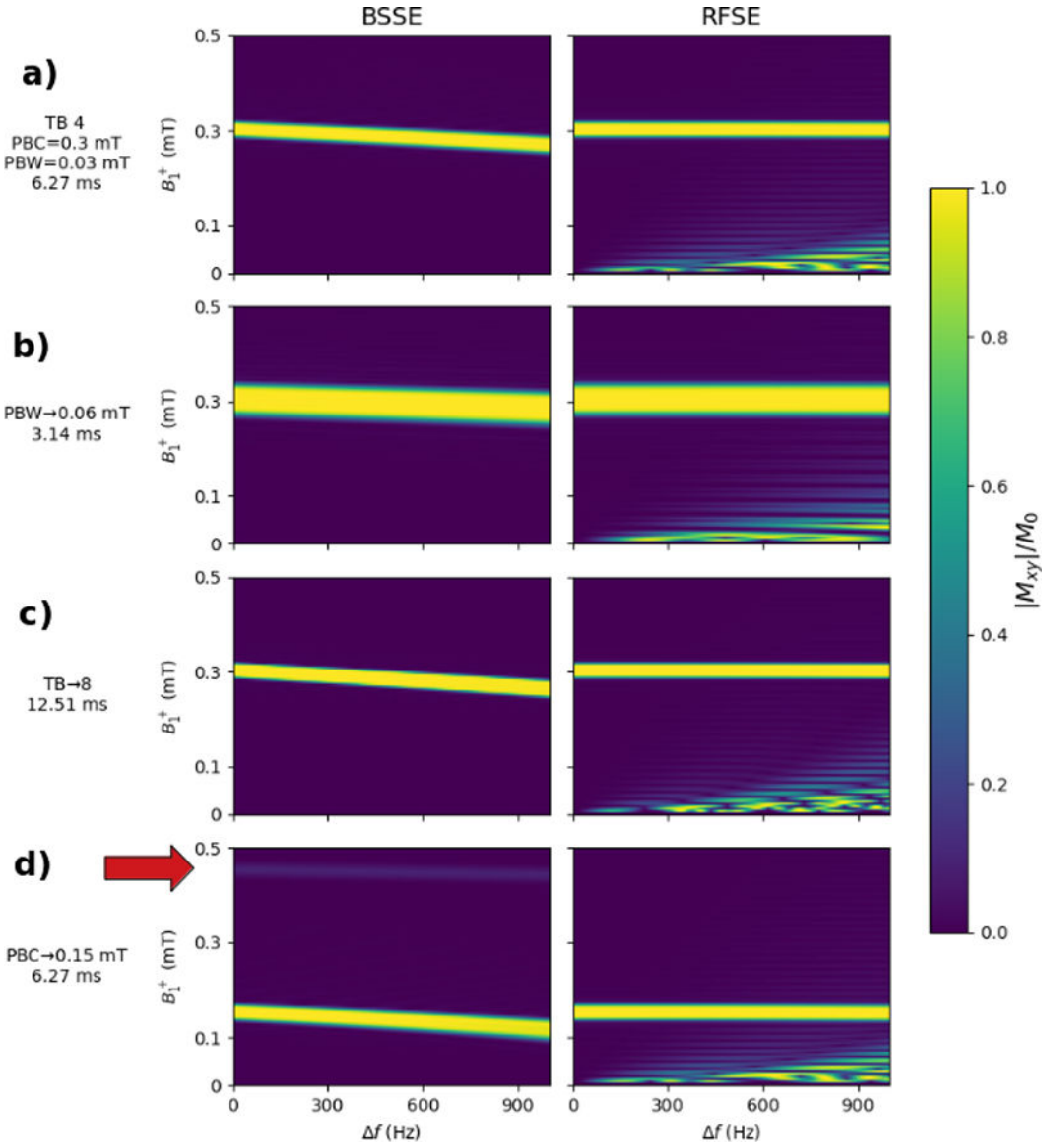

Figure 7.

Simulations of BSSE and RFSE pulse off-resonance sensitivity. a) Simulation of the "base" 6.27ms BSSE and RFSE pulses with TB=4, PBC=0.4 mT, PBW=0.03 mT, FA=90°. ω_{off} was set to 16.37 kHz to match the RFSE pulse duration. b) Same as base pulse but with PBW set to 0.06 mT. ω_{off} was set to 9.48 kHz to match durations. c) Same as base but with TB set to 8. ω_{off} was set to 19.25 kHz to match durations. d) Same as base but with PBC set to 0.15. ω_{off} was set to 8.17 kHz to match durations. In all cases, the BSSE magnetization profiles show a bulk shift in the magnetization profile with increasing off-resonance. The red arrow in d) shows the location of an $N = 3$ multiphoton resonance. This multiphoton resonance also experiences a bulk shift downward in B_1^+ with increasing off-resonance. The RFSE profiles show no bulk shift, but have substantial unintended excitation at low B_1^+.

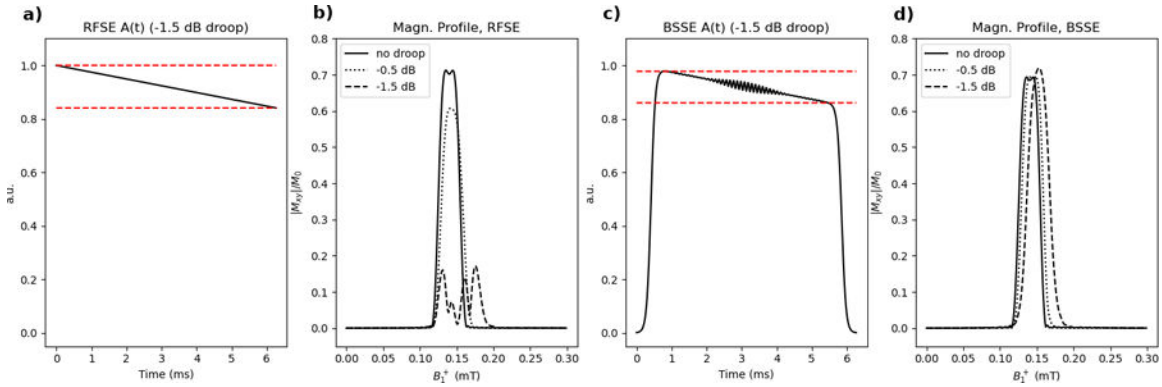

Figure 8.

Simulation of RF amplifier droop. AM waveforms for RFSE (a) and BSSE (c) RF pulses are shown with −1.5dB of droop. In the case of the RFSE pulse, the magnetization profile (b) is severely degraded by RF amplifier distortion. However, the magnetization profile of the BSSE pulse (d) experiences only a slight shift upward in B_1^+, with minimal profile distortion.

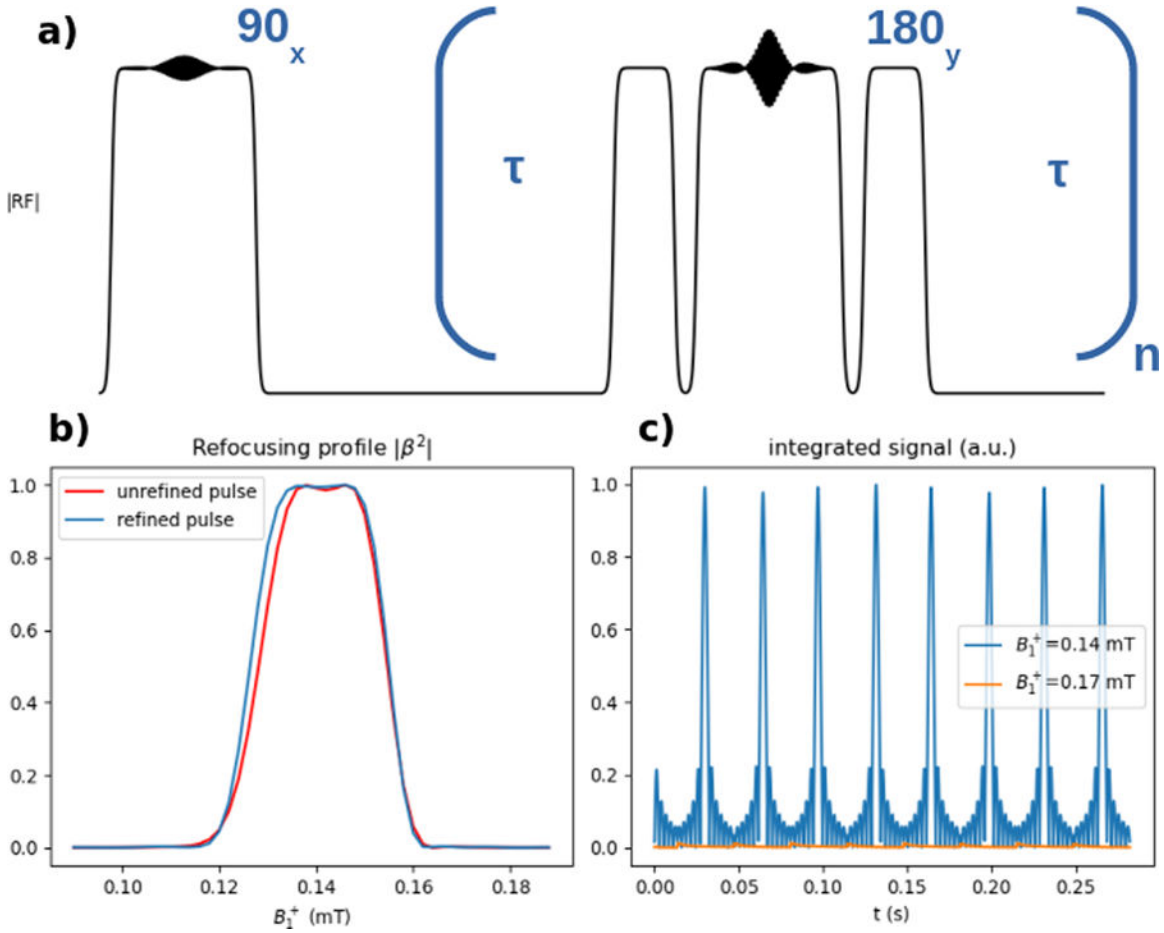

Figure 9.

BSSE Multi-echo CPMG pulse sequence. a) Pulse sequence diagram. A 90° excitation pulse was followed by a train of 180° pulses. To satisfy the CPMG phase conditions, RF pre- and re-winders were inserted before and after the 180° refocusing pulses. b) $|\beta^2|$ refocusing efficiency profile for the refocusing pulse. Refocusing was selective and nearly complete across the passband. The gradient descent-refined 180° pulse had a slightly improved profile, although the unrefined pulse also performs well given the narrow PBW. c) Signal timecourse in the passband and stopband. Regularly spaced echos of uniform amplitude were produced in the passband.

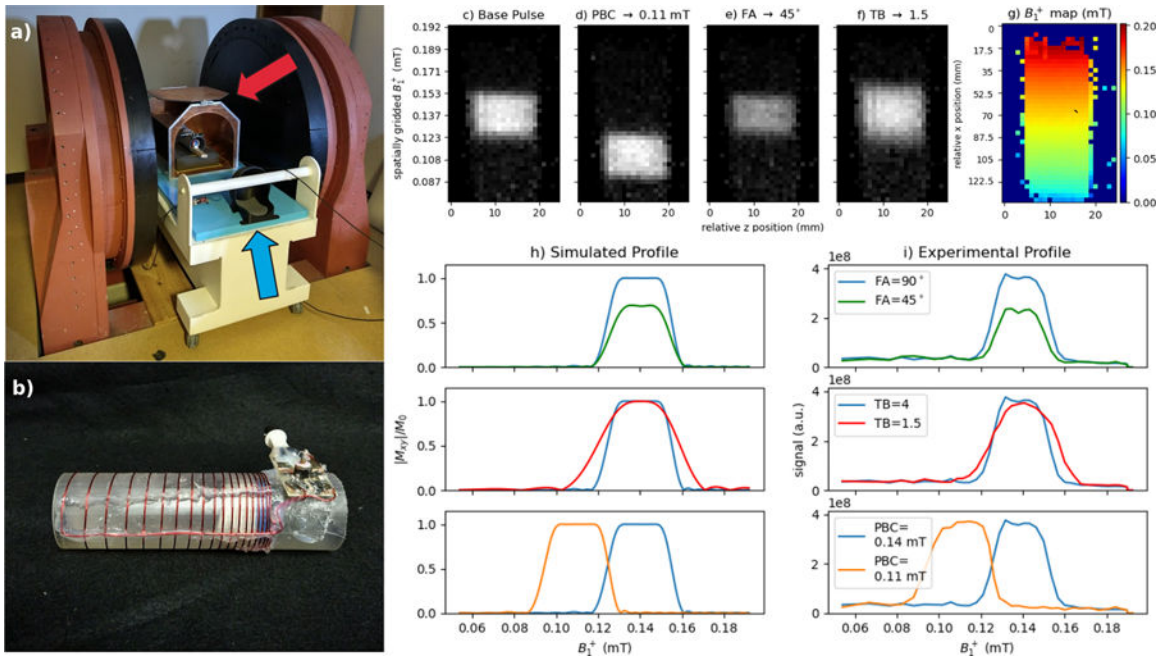

Figure 10.

a) 47.5 mT permanent magnet system used for experimental results. A Faraday cage (red arrow) and pickup coil (blue arrow) are used to reduce EMI. b) variable-pitch T/R solenoid coil used in experiments. The tube phantom is placed inside in this image. c-f) middle slice of 3D GRE acquisition with varying BSSE excitation pulse. g) B_1^+ map corresponding to the same slice h) 1D simulated profiles for the pulses, and i) corresponding experimental 1D profiles. The 45° excitation (green) produces reduced signal intensity in relation to the 90° excitation (blue). The TB=1.5 excitation (red) produces a profile with a broader transition region. Designing the pulse with PBC shifted to 1.1 G (orange) produces the corresponding change in the magnetization profile.